BIOCHEMISTRY
including biophysical chemistry & molecular biology

Article

pubs.acs.org/biochemistry

Looking at Human Cytosolic Sialidase NEU2 Structural Features with an Interdisciplinary Approach

Eugenio Monti,*[,†] Giuliana Benaglia,[†] Alessandra Mozzi,[‡] Paola Fusi,[‡] Giovanna Longhi,[†,§] Fabrizio Gangemi,[†] Ettore Castiglioni,[†,∥] Robert W. Woody,[⊥] Sandro L. Fornili,[#] and Sergio Abbate[†,§]

[†]Department of Molecular and Translational Medicine (DMTM), University of Brescia, Viale Europa 11, 25123 Brescia, Italy
[‡]Department of Biotechnology and Bioscience, University of Milano-Bicocca, Piazza della Scienza 2, 20126 Milano, Italy
[§]CNISM Consorzio Nazionale Interuniversitario per le Scienze Fisiche della Materia, Via della Vasca Navale, 84, 00146 Roma, Italy
[∥]JASCO Europe, via Cadorna 1, 23894 Cremella (LC), Italy
[⊥]Department of Biochemistry and Molecular Biology, Colorado State University, Fort Collins, Colorado 80523, United States
[#]Department of Informatics, University of Milan, Via Bramante 65, 26013 Crema (CR), Italy

Supporting Information

ABSTRACT: Circular dichroism (CD) spectra at variable temperatures have been recorded for human cytosolic sialidase NEU2 in buffered water solutions and in the presence of divalent cations. The results show the prevalence of β-strands together with a considerable amount of α-helical structure, while in the solid state, from both previous X-ray diffraction analysis and our CD data on film samples, the content of β-strands is higher. In solution, a significant change in CD spectra occurs with an increase in temperature, related to a decrease in α-helix content and a slight increase in β-strand content. In the same range of temperatures, the enzymatic activity decreases. Although the overall structure of the protein appears to be particularly stable, molecular dynamics simulations performed at various temperatures evidence local conformational changes possibly relevant for explaining the relative lability of enzymatic activity.

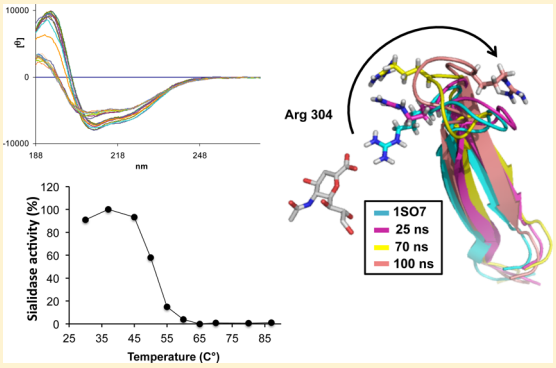

Sialidases or neuraminidases (EC 3.2.1.18) are glycohydrolases that remove α-glycosidically linked sialic acid residues from the terminal position of glycoprotein and glycolipid saccharide moieties.[1] These enzymes are widely distributed in nature, from lower metazoans to mammals;[2] microorganisms, including fungi, protozoa, and bacteria, even most of those lacking sialic acids; and also various viruses.[1] The relevance of sialidase in influenza virus biology boosted the research on this class of glycohydrolases, leading to the determination of several neuraminidase three-dimensional structures and the development of competitive inhibitors as drugs for fighting the war against influenza.[3]

From a structural point of view, viral and microbial sialidases are found in monomeric, dimeric, and tetrameric forms, the monomer showing a typical six-blade β-propeller structure.[4] The crystal structures of human cytosolic sialidase NEU2 in its apo, sugar-induced form and as a complex with the competitive inhibitor 2-deoxy-2,3-dehydro-*N*-acetylneuraminic acid [DANA (Figure 1A)] further demonstrate, despite the low degree of similarity that can be detected between the amino acid sequences of bacterial enzymes and the human counterpart, the high degree of conservation of the six-blade β-propeller.[5]

Briefly, NEU2 exhibits the typical six blades (indicated by roman numerals I–VI) of the β-propeller, each composed of four antiparallel β-strands (indicated by capital letters A–D) (Figure 1B). The β-propeller is closed by the interaction between strands C and D of blade VI, with the element of β-strand D belonging to the N-terminus (amino acids 8–14) of the polypeptide. The antiparallel β-strands are connected by amino acid stretches of various lengths and secondary structures (i.e., unordered, turns, or helices). The N- and C-termini, consisting of 7 and 12 residues, respectively, are on the external surface of the β-propeller and are located close to each other. In addition, on the surface of the β-propeller are three so-called Asp boxes, a motif (Ser X Asp X Gly X X Trp/Phe) typical of sialidases.[6] Asp boxes form well-defined β-hairpins located in topologically equivalent positions between strands C and D of blades II–IV and are thought to play a structural role in the β-propeller.[7] An acidic crevice at the center of the β-propeller forms the active site with conserved residues involved in the catalytic process; on the opposite side of the β-propeller, an acidic deep cleft extends very close to the bottom of the catalytic site (Figure 1). Intriguingly, enzymatic activity has been established to be influenced by the presence of divalent cations, in particular Ca^{2+}.[8,9] With regard to

Received: February 26, 2014
Revised: June 25, 2014
Published: July 17, 2014

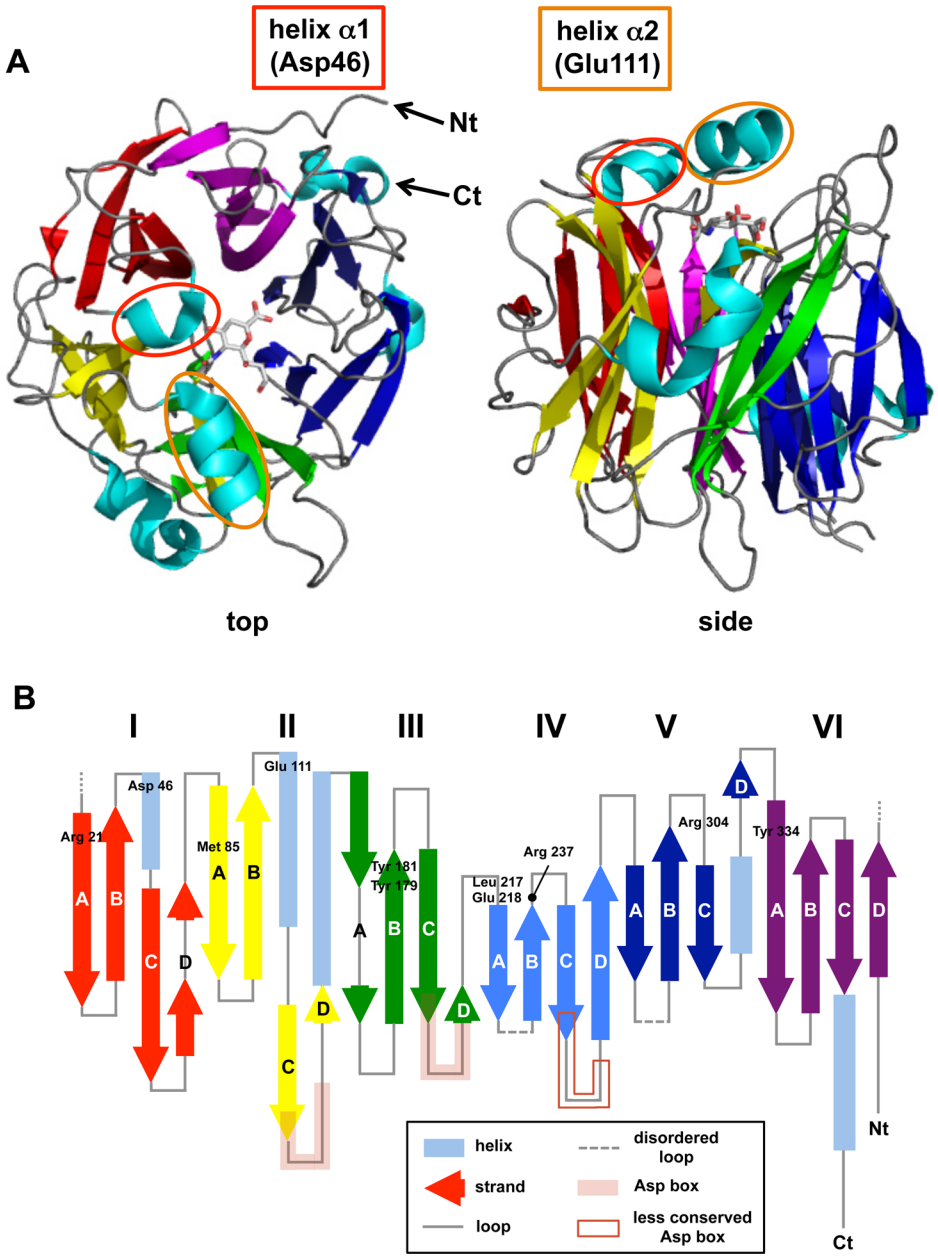

Figure 1. (A) Ribbon diagram of human cytosolic sialidase NEU2 as a complex with the competitive inhibitor DANA and derived from the X-ray structure of Protein Data Bank entry 1VCU. The mobile loops containing helices α1 and α2 are encircled by red and orange ovals, respectively. (B) Schematic diagram of the NEU2 β-propeller topology, evidencing the six blades of the propeller (I–VI), each one, apart the second, formed by four antiparallel β-strands (A–D) and the other structural features of the protein. Nt and Ct stand for the N-terminus and C-terminus of the polypeptide, respectively.

the organization of the active site, NEU2 contains several residues that appear to be highly conserved in the family of viral and microbial sialidases and are organized in a shallow crevice at the center of the propeller[10] [Figure 2, where the competitive inhibitor 2-deoxy-2,3-dehydro-*N*-acetylneuraminic acid (DANA) is also shown].

Among these, Glu 218 and Tyr 334 are located at the bottom of the active site and represent the nucleophile pair required for catalysis,[10,11] Arg 21, Arg 237, and Arg 304 represent the Arg triad that allows binding of the C1 carboxyl group of sialic acid (Figure 2), and Met 85 and Tyr 179, Tyr 181, and Leu 217 are involved in the recognition of the *N*-acetyl group and the glycerol tail of the acidic sugar, respectively. The unique structural feature of NEU2 is the presence of two mobile loops between strands B and C of blades I and II of the β-propeller (Figures 1 and 2). These connecting stretches of residues are disordered in NEU2 apo form [Protein Data Bank (PDB) entry 1SNT], while the soaking of crystals with a monosaccharide such as galactose, glucose, or maltose orders the loop of the second blade (PDB entry 1SO7). Finally, the structure of NEU2 in complex with the competitive inhibitor DANA obtained by cocrystallization (PDB entry 1VCU) demonstrates a rearrangement of the second blade loop that is now bent close to the *N*-acetyl and glycerol portion of DANA and, at the same time, the loop of the first blade becomes ordered and is positioned near the C4 hydroxyl group of the competitive inhibitor.[5] Moreover, these loops connecting antiparallel β-strands contain two of the seven short α-helices found in NEU2, namely, α1 and α2, and two acidic residues (Asp

dx.doi.org/10.1021/bi500249r | *Biochemistry* 2014, 53, 5343–5355

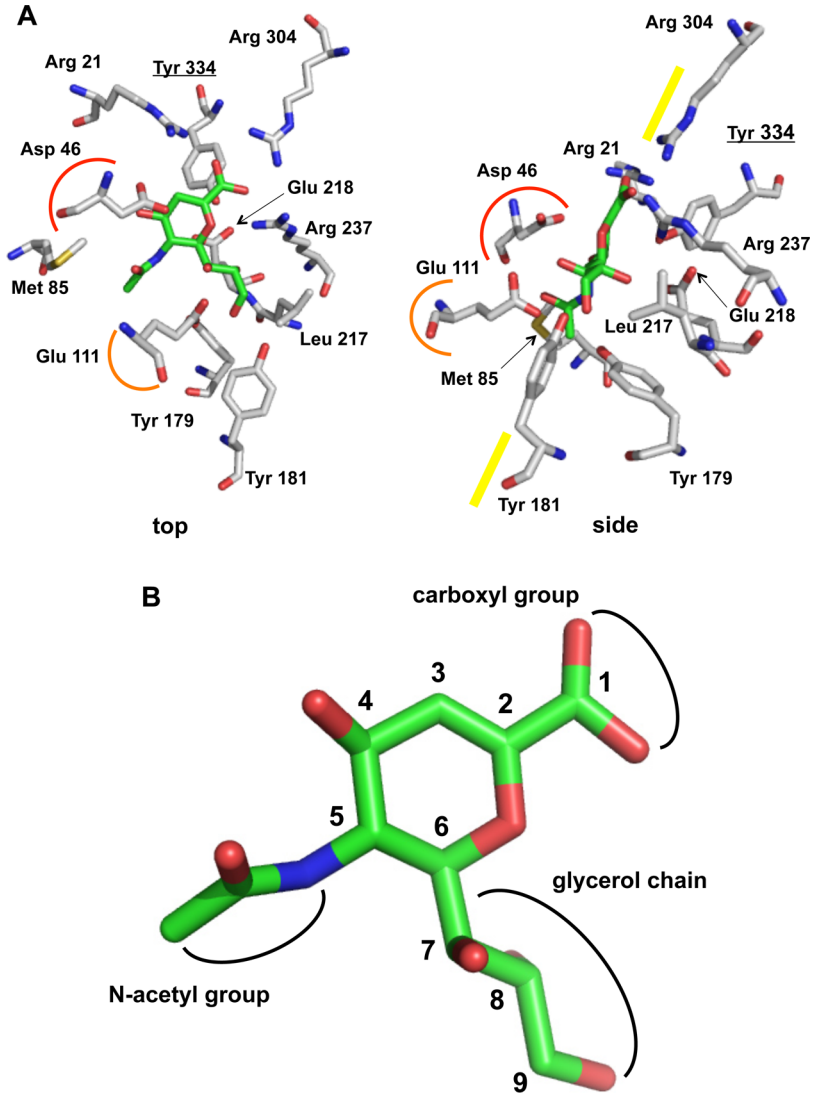

Figure 2. Positions of the amino acid residues in the active site crevice of NEU2. (A) Top and side views of the residues involved in DANA coordination. Asp 46 (red semicircle) and Glu 111 (orange semicircle) are within helices α1 and α2, respectively, and belong to highly mobile loops connecting antiparallel β-strands B and C of blades I and II of the β-propeller (Figure 1B). Tyr 334 is underlined because of its pivotal role in the catalysis (see the text for more details). Yellow lines indicate the plane of the DANA pyranose ring. (B) Structure and group numbering of 2-deoxy-2,3-dehydro-*N*-acetylneuraminic acid (DANA), provided to facilitate discussion in the text.

46 and Glu 111, respectively) involved in DANA coordination. From this perspective, when DANA binds and, possibly, in the binding process of more complex oligosaccharides, which are the natural substrates of the enzyme, the two loops containing Asp 46 and Glu 111 bend over the active site crevice and partially cover the inhibitors (Figure 1 and 2), demonstrating the dynamic nature of substrate recognition.[5]

The aim of this work is to gain information about the NEU2 structure in aqueous solution, a condition that is supposed to mimic the enzyme function within the cytosol better than the crystal. The main experimental method employed is circular dichroism (CD), an easy to use technique that has been used for a long time for protein secondary structure determination.[12−18] The CD study has been conducted as a function of temperature also in the presence of ions, possibly involved either directly or indirectly, inhibiting or promoting catalytic activity. In parallel, we have tested the catalytic activity by conducting a standard fluorimetric enzyme assay. In addition, molecular dynamics (MD) simulations have been conducted, aiming to formulate reasonable hypotheses at the atomic level about the significance of observed spectroscopic and biochemical data.

EXPERIMENTAL AND COMPUTATIONAL DETAILS

Protein Preparation, Purification, and Biological Assays. Human cytosolic sialidase NEU2 has been obtained as a recombinant enzyme starting from *Escherichia coli* DH5α cells transfected with pGEX-2T-NEU2 as previously described.[8] Briefly, cells were harvested by centrifugation and suspended in 50 volumes of phosphate-buffered saline (PBS). Cells lysed by sonication and supernatants obtained after centrifugation at 12000*g* for 10 min were assayed for sialidase activity. Purification of the GST−NEU2 fusion protein was conducted by affinity chromatography on a GSH-Sepharose 4B column according to the manufacturer's instructions (GST Gene Fusion System, GE Healthcare Bio-Sciences), with minor modifications. After an additional washing with PBS and 0.5 M NaCl, cleavage of the GST moiety from the protein chimera bound to the matrix was conducted by adding 0.5 IU of thrombin/mL of gel bed volume

dx.doi.org/10.1021/bi500249r | *Biochemistry* 2014, 53, 5343−5355

(GE Healthcare Bio-Sciences) in PBS and incubating the column for 2−3 h at room temperature. The resulting enzyme was divided into aliquots and stored at −80 °C until it was used in 10 mM KH_2PO_4 (pH 7.4) (phosphate buffer, called PB) to permit subsequent optimal CD measurements without spectroscopic interference from salt such as NaCl. For CD measurements in the presence of divalent ions, $CaCl_2$ or $CuCl_2$ was added to PB to a final concentration of 3.5 or 0.7 mM, respectively.

The enzymatic activity was tested using the artificial fluorescent substrate 4-methylumbelliferyl-α-D-*N*-acetylneuraminic acid (4-MU-NeuAc) (Sigma), which is hydrolyzed by the enzyme to NeuAc and 4-methylumbelliferone (4-MU). The presence of the 4-MU reaction product was detected under alkaline conditions using a spectrofluorimeter (Jasco FP-770, Jasco Europe), with excitation at 365 nm and emission at 445 nm, using 4-MU to set up a calibration curve. The reaction mixtures (100 μL) prepared at pH 5.6 (25 mM Na citrate/phosphate buffer) with an appropriate concentration of 4-MU-NeuAc (0.1 mM) in the presence of 20 μg of bovine serum albumin were incubated at 37 °C with purified recombinant NEU2 (1 μg) for up to 10 min. Finally, enzyme reactions were stopped by the addition of 1.5 mL of 0.2 M glycine-NaOH (pH 10.2).

CD and IR Spectroscopy. CD spectra were recorded on a Jasco J-815SE spectropolarimeter for solutions with concentration of ≥0.17 mg/mL, contained in a 1 mm quartz cylindrical jacketed cell, thermostated by external-circuit water flow. Spectra were recorded for each temperature at a rate of 100 nm/min, with a response time (τ) of 2 s; the baseline of the buffer has been subtracted from each spectrum. A 10 min time interval between two spectra for two different temperature values (generally each 2.5 °C) was assured. CD spectra were also recorded at room temperature on films grown on a quartz window from buffered KH_2PO_4 solutions. We made sure that the sample was kept close to the detector, to reduce scattering effects. In addition, four measurements were performed and averaged, changing the window orientation at 0° and 90° and collecting spectra with the film on the same side or opposite the source, to compensate for possible artifacts from linear dichroism and birefringence, potentially present in solid-state CD measurements.[19] The mean residue ellipticity was evaluated, for the analysis of the secondary structure, assuming an extinction coefficient at 280 nm of 57500 M^{-1} cm^{-1}, as calculated in Prot-Param-Toolbox (http://web.expasy.org/protparam/), and considering 111.13 amu as the mean residue mass, namely the total mass (42230.6) divided by the number of residues (380).

To gain further information about solid samples, we recorded IR spectra on a similar film grown on a ZnSe window. We used a Jasco FVS4000 spectrometer, equipped also with the VCD module, but we limited ourselves to IR spectra; for this reason, just 100 scans were taken.

MD Simulations. MD simulations were conducted by means of GROMACS 4.5[20] with the amber99SB force field.[21−23] The initial molecular model was derived from one of the X-ray structures (PDB entry 1SO7)[5] available in the Protein Data Bank.[24] Missing residues were added by means of Swiss PDB Viewer,[25] and the choice among different possible conformations was based on Ramachandran angles and energies.[26] Following the X-ray structure, a disulfide bond was also imposed between residues Cys 88 and Cys 164 while building the input topology file. The protein was solvated by adding TIP3P water molecules in an octahedral box, imposing a minimal distance of 10 Å between the solute and the boundary of the solvent box. This resulted in approximately 19400 water molecules. Sodium ions were added to neutralize the system, because the protein has a net charge of −3*e* at neutral pH, as determined by the GROMACS preprocessing routines. Further ions were added to comply with the different experimental situations to be simulated. We use the shorthand notation *ss* (salt solution) to indicate the situation in which the solvent box contains 60 Na^+ ions and 57 Cl^- ions, corresponding to a salt concentration of approximately 160 mM. In other simulations, labeled as "Ca" and "Cu", we also included 10 Ca^{2+} ions and 10 Cu^{2+} ions, respectively, and 20 more Cl^- ions in both cases to balance the extra positive charge. The parameters of Ca^{2+} ions are available in the standard force field, while those of Cu^{2+} were taken from Table 5 of ref 27. Electrostatic interactions were calculated according to the particle mesh Ewald (PME) algorithm, with a cutoff of 10 Å. A cutoff of 14 Å was used for the van der Waals interactions. For each simulation, 5000 steps of steepest-descent minimization were initially performed, followed by equilibration phases at 300 K for 20 ps at a constant volume and 40 ps at a constant pressure (1 bar), with position restraints on the solute. Then the system without restraints was simulated at constant pressure and temperature with a time step of 2 fs, and the atomic coordinates were collected every picosecond. Velocity rescaling was used to control the temperature, with a time constant (τ_T) of 0.1 ps, and the Parrinello−Rahman algorithm[28,29] to control the pressure, with τ_P = 1 ps and a compressibility of 4.5×10^{-5} bar^{-1}. All bonds were constrained by means of the LINCS algorithm.[30]

For simulations above 300 K, the final state of the equilibration process at 300 K was taken as the starting conformation for the heating phase in which the temperature was linearly increased in a time interval of 100 ps (200 ps in the case of 500 K), followed by equilibration for 100 ps without restraints at the higher temperature. Multiple simulations with different initial conditions (namely, Maxwellian velocity distribution of all atoms and initial positions of ions) were performed at 300 K, for a total of 200 ns in the *ss* case and in the "Cu" case, and 250 ns in the "Ca" case. Simulations at 348 and 358 K had a length of 50 ns each, and the *ss* simulations at 500 K had a length of 100 ns. Two simulations, one at 348 K for 100 ns and one at 300 K for 50 ns, denoted in the following as simulated annealing (s.a.), were performed after that at 500 K. The transition to 348 K was performed in six linear 1 ns steps, each followed by 10 ns at a constant temperature. The subsequent decrease in temperature to 300 K was done in three linear 1 ns steps, each followed by 5 ns at a constant temperature.

Standard trajectory analyses were performed by means of the GROMACS routines. The *B* factor per residue was calculated as the mass-weighted average of atomic *B* factors of atoms other than hydrogen in the same residue:

$$B = (8\pi^2/3)[\sum m_i(x_{ij} - \langle x_{ij}\rangle)^2/\sum m_i]$$

where x_{ij} is Cartesian component *j* of atom *i*, $\langle x_{ij}\rangle$ is its average value, and m_i is the mass of atom *i*. The secondary structure was analyzed using the GROMACS utility based on DSSP.[31,32] According to the latter, the secondary structures are classified as coil, β-sheet, β-bridge, bend, turn, α-helix, π-helix, and 3_{10}-helix. To compare the results with those obtained from experimental data (Jasco SSE software for secondary structure estimation from CD spectra, Jasco Inc., Tokyo, Japan), we grouped the DSSP results as follows: U (coil), S (β-sheet or β-bridge), T (bend or turn), and H (α-helix, 3_{10}-helix, or π-helix, the last being of negligible importance in all cases studied here). Average numbers of ions close to protein residues were calculated by integrating

over a spherical volume with a radius r_0 of 10 Å the radial distribution functions $g(r)$, evaluated with respect to the center of mass of each residue, and multiplying by the number density ρ of ions: $N_i = \rho \int 4\pi r^2 g(r)\, dr$. We chose the hydrogen-bond (HB) definition that requires an acceptor−donor−hydrogen angle <30° and a donor−acceptor distance of <3.5 Å. The HB time evolution was calculated every 10 ps and displayed with a running average over 200 ps to obtain readable graphics. We also employed a previously implemented program[33] to evaluate principal moments of inertia of the protein. On the basis of the so-called matrix method,[34−36] calculations of the CD spectra were performed using PROTEIN and PROTPOL developed by R. W. Woody and N. Sreerama.[37−39] Visual analysis of molecules was conducted using VMD[40] and PyMOL (The PyMOL Molecular Graphics System, MacPyMOL: PyMOL Enhanced for Mac OS X, DeLano Scientific LLC).

RESULTS AND DISCUSSION

As outlined in the introductory section, the three-dimensional structure of crystallized NEU2 has been previously investigated by X-ray diffraction in three forms, namely, apo, maltose-induced, and DANA−NEU2 complex[5] (other NEU2 complexes with various competitive inhibitors acting as anti-flu drugs were studied by X-ray[41]). To further study the structural features of NEU2 in the solid-state phase by a quite independent method, we have measured CD (in the far UV) and IR spectra (between 1400 and 1800 cm^{-1}) of film samples at room temperature. We note that the NEU2 film employed for conducting CD measurements may not provide a condition identical to that found in X-ray experiments, but it assures acquisition of CD data safe from distortions of CD curves due to either scattering or absorption flattening and from artifacts due to birefringence and linear dichroism. Results are reported in Figure 3: the CD features are indeed immediately recognized, on a qualitative basis, as being indicative of β-strands (S).

On the basis of current methods[13,15−18] (Jasco SSE software for secondary structure estimation from CD spectra, Jasco Inc.), statistical analysis of the spectrum was also conducted by calculating mean residue ellipticities from the data reported in Figure 3, through knowledge of absorption data in the aromatic region. Thus, we found that S motifs are predominant, but not exclusive (Table 1, film).

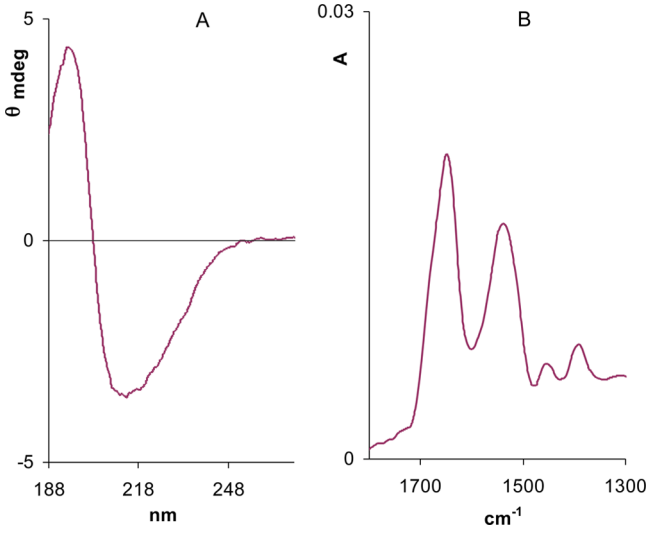

Figure 3. (A) Circular dichroism (CD) spectrum of NEU2 in the solid state (film sample on a quartz support). (B) IR spectrum of NEU2 in the solid state (film sample on a ZnSe support). For further details of the experiments, see the text.

Table 1. Percentages of Secondary Structures As Obtained from the X-ray Structure[5] and from the Analysis of CD Spectra at Two Temperatures (17.5 and 85 °C) with CDSSTR[15,16] (top) and CONTIN-LL[13,16] (bottom) Methods

	H	S	T	U
X-ray	9%	46%	23%	22%
CDSSTR				
film	5%	39%	25%	31%
K at 17.5 °C	20%	30%	20%	30%
Cu at 17.5 °C	18%	31%	21%	29%
Ca at 17.5 °C	17%	31%	22%	30%
K at 85 °C	7%	35%	25%	33%
Cu at 85 °C	5%	35%	26%	34%
Ca at 85 °C	4%	37%	27%	32%
CONTIN-LL				
film	8%	39%	22%	31%
K at 17.5 °C	22%	28%	22%	28%
Cu at 17.5 °C	21%	29%	21%	29%
Ca at 17.5 °C	19%	29%	23%	29%
K at 85 °C	12%	32%	23%	33%
Cu at 85 °C	9%	37%	22%	32%
Ca at 85 °C	6%	18%	28%	48%

Actually, S motifs amount to 39%, while turn motifs (T) and unordered (U) motifs are less abundant (~22−25 and ~31%, respectively); as expected from the crystal structure (Figure 1), ~5−8% helical structure (H) is also present. It is worth noting that CD spectra were analyzed using two different programs to provide reliability ranges of these methods. Besides, on the basis of the work of Sreerama and Woody,[16] rms errors of 8% for H, 9% for S, 8% for T, and ~12% for U can be anticipated. Considering the IR spectrum, the analysis of the amide I band[42] centered at 1650 cm^{-1} by statistical weights of principal components[43,44] gives a high percentage of S and U (27% each) and a significant amount of T and H (25 and 21%, respectively). The percent contents of secondary structures derived from film CD data are more similar to those observed with X-ray than IR data (Table 1).

To determine whether other conformations with possible biological relevance emerge in solution, we have run CD spectra of NEU2 in PB or with addition of divalent cations ($CuCl_2$ or $CaCl_2$), which have been shown to influence the catalytic activity measured at 37 °C.[8,9] Spectra were recorded in the temperature range of 15−90 °C (Figure 4).

Three facts emerge from the analysis of CD spectra. (1) Spectra cluster in two sets with a clearly noticeable and steep variation, especially in the case of PB, which suggests a transition between two types of arrangements in the secondary structure. (2) The overall shape of the CD spectrum is different from that observed in the solid state, exhibiting a doublet in the negative feature, which is reminiscent of α-helix behavior.[12,14,17,18] In addition, the positive maximum at ~194 nm, detectable in the solid state as well, is typical of α-helix structures as well as β-sheet. When samples are heated, these features change in intensity, wavelength, and shape. To better evidence the temperature dependence of this spectral variation, in Figure 5 we plot the CD intensity as a function of temperature for three characteristic features, namely, the two negative features at 222 and 208 nm

dx.doi.org/10.1021/bi500249r | Biochemistry 2014, 53, 5343−5355

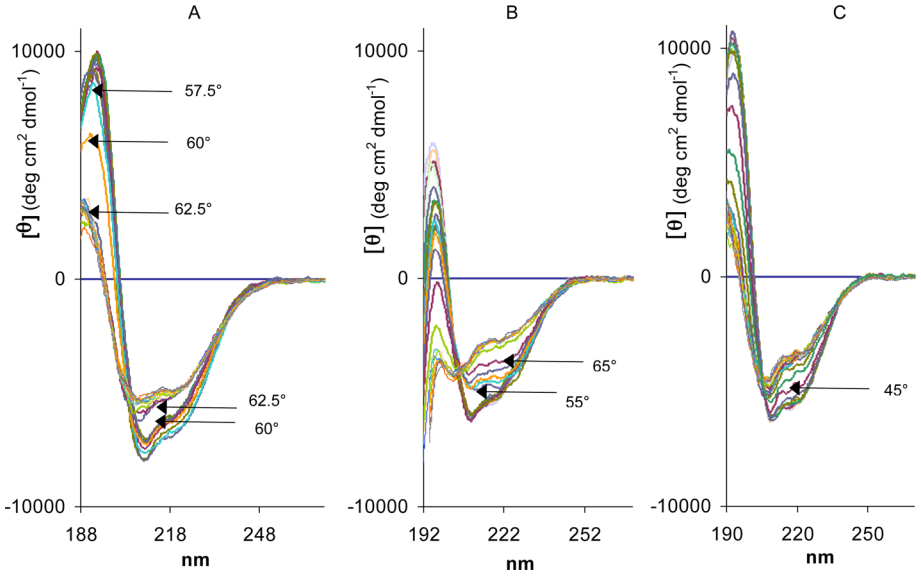

Figure 4. (A) Variable-temperature circular dichroism spectra of NEU2 in PB (see the text) in the temperature range of 15−90 °C. (B) CD spectra of NEU2 in PB in the presence of $CaCl_2$ in the temperature range of 15−90 °C. (C) CD spectra of NEU2 in PB in the presence of $CuCl_2$ in the temperature range of 15−90 °C. For further information, see the text.

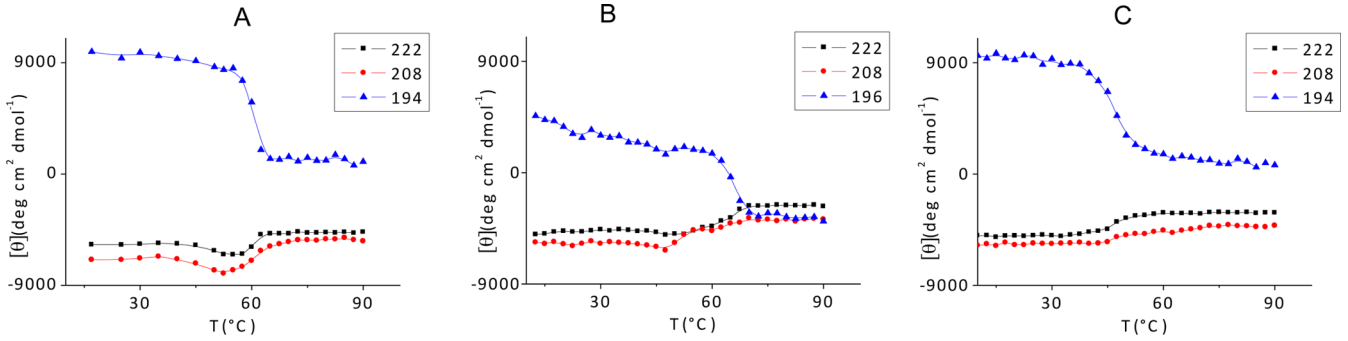

Figure 5. (A) CD intensities in mean residue ellipticity (MRE) units vs temperature at the fixed wavelengths, reported in the inset, for the spectra of Figure 4A (PB solution). (B) MRE vs temperature at fixed wavelengths, reported in the inset, for the spectra of Figure 4B (PB and $CaCl_2$). (C) MRE vs temperature at fixed wavelengths, reported in the inset, for the spectra of Figure 4C (PB and $CuCl_2$).

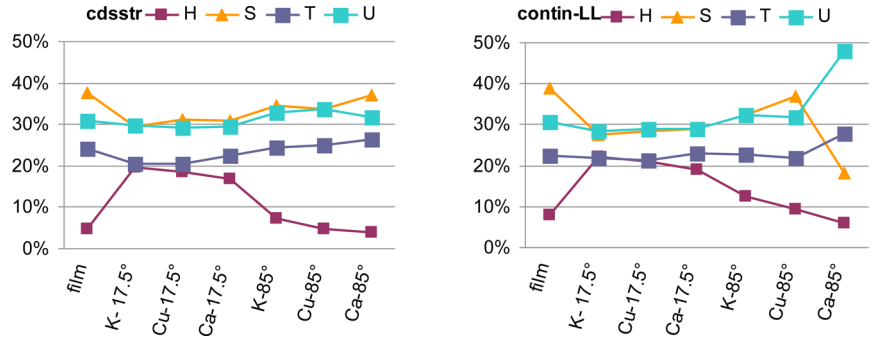

Figure 6. Pictorial comparison of the percentage contents of the different components evaluated in Table 1 by using CDSSTR and CONTIN-LL programs for the various samples of NEU2 investigated at room temperature and at a temperature above the observed transition. For further information, see the text.

and the positive maximum found at 194 nm for PB and Cu^{2+} and at 196 nm for Ca^{2+}. This representation of the CD data allows definition of the third important point mentioned above. (3) The thermal variations are different in the three cases. In fact, a rather sharp transition between 55 and 65 °C ($T_m \sim 60$ °C) is found for NEU2 in PB (Figure 5A), which covers the same, or a slightly larger, interval in the presence of Ca^{2+} ions ($T_m \sim 65$ °C) (Figure 5B) and decreases to the range of 45−55 °C in the presence of Cu^{2+} (Figure 5C).

The same statistical analysis of the CD spectra as employed for solid-state CD data has been conducted with spectra recorded in solution and has yielded the results summarized in Table 1. Moreover, an overall view of the same data is given in Figure 6. At room temperature, the content of β-strands (S) is slightly lower,

dx.doi.org/10.1021/bi500249r | Biochemistry 2014, 53, 5343−5355

if compared with that of the solid film, in favor of α-helix (H), while the U content is, as already reported, increased in both film and solution compared to X-ray and persists at 30%. It is tempting to associate the increase in H content with the loops connecting the β-strands undergoing the coil → helix transition, but the data presented here are not enough to draw such a conclusion. When the change has taken place, above the T_m, the H content decreases again, in favor of unordered U and T protein secondary structures. Intriguingly, the graphics in Figure 6 clearly show that at higher temperatures most of the secondary structural motifs of the overall protein conformation appear to approach the same values observed in the solid state. Similar evidence from CD spectra has been found in the presence of molecules that can interact with the active site such as glucose and maltose, sialic acid, or DANA, while the whole CD spectrum has been observed to be altered irreversibly in the presence of denaturing agents like SDS (data not shown).

At this point, an investigation of NEU2 enzymatic activity as a function of temperature was conducted to find a possible correlation with the CD experiments. The results indicate a steep decrease in enzyme activity starting from 45 °C, with an almost complete loss of catalytic power at 60 °C (Figure 7). This temperature range roughly corresponds to the transition temperature observed in CD experiments (Figures 4 and 5).

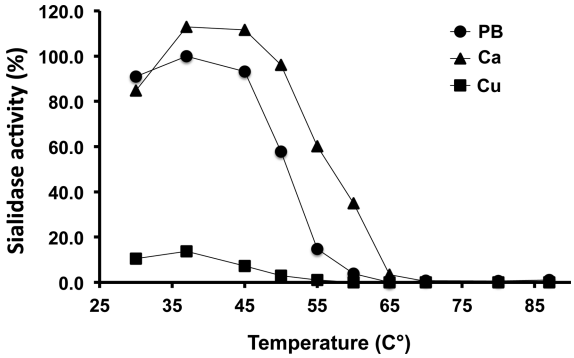

Figure 7. Enzymatic activity of NEU2 vs temperature. The activity is assayed in terms of nanomoles of 4-methylumbelliferone (4-MU) per liter released by the enzyme hydrolytic action on 4-methylumbelliferyl-α-D-*N*-acetylneuraminic acid (4-MU-NeuAc) and reported as the percentage of the maximal value observed with NEU2 in PB without divalent cations. The activity curves of NEU2 measured in the presence of 3.5 mM $CaCl_2$ and 0.7 mM $CuCl_2$ are also shown. For further information, see Experimental and Computational Details.

The effects of Ca^{2+} and Cu^{2+} on enzymatic activity as a function of temperature are quite different. Calcium shows a slight activating effect and appears to protect NEU2 from heat inactivation, with a roughly 5−10 °C upward shift of the temperature values at which the enzyme activity starts to decrease. Conversely, copper at the same concentration, 7 mM, strongly inhibits the enzyme activity that is almost completely abolished at 55 °C. These results are in good accordance with the shift in the transition temperature observed in CD spectra (Figures 4C and 5C). However, the enzyme activity has been shown to be unstable after the sample has thawed from −80 °C, even if the protein sample is maintained at 4 °C.[8] This behavior of the enzyme could be related to subtle structural variations that result in a decrease in measurable catalytic activity.

To gain further insight into the atomic-level properties of NEU2 in aqueous solution and the involvement of divalent cations, MD simulations were performed at various temperatures and solvent compositions. It is worth noting that, because of the high rigidity of β-propeller structures,[45−47] large structural changes such as those evidenced by the variations of CD spectra with temperature might be outside the reach of typical simulation times (hundreds of nanoseconds). Nevertheless, MD simulations could help reveal some local atomic-scale processes underlying the system macroscopic behavior.

For the simulations at 300 K of the *ss* solution, the time evolution of the root-mean-square deviation (RMSD) of Cα atoms with respect to the X-ray structure (Figure 8A) shows that

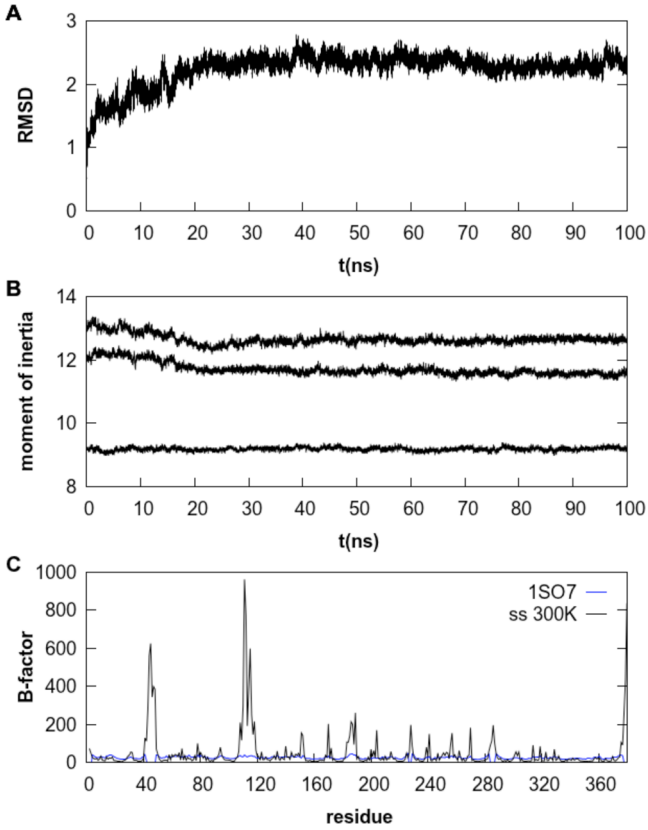

Figure 8. (A) Root-mean-square deviation (RMSD, Å) of the Cα atoms evaluated by MD for human cytosolic sialidase NEU2 with respect to the crystallographic structure in 100 ns simulations at 300 K in the presence of *ss* (for details, see the text). (B) Principal moments of inertia (in 10^6 atomic mass units per square angstrom) of NEU2 evaluated by MD as a function of time in 100 ns simulations at 300 K in salt solution (*ss*). (C) *B* factor (square angstroms) evaluated for each residue of NEU2 in PDB entry 1SO7 and in 100 ns MD simulations at 300 K in *ss*. For further information, see the text.

within ∼20 ns a rather stable value on the order of 2 Å is reached, indicating that the structure as a whole is quite rigid. In the same time interval, the overall shape of the protein, as described by the principal moments of inertia, also becomes nearly constant along the trajectory (Figure 8B).

However, the analysis of the *B* factor (Figure 8C) shows different degrees of mobility in different parts of the sequence: a higher mobility is found, as expected, in the region close to the C-terminus, and mainly in regions surrounding the protein active site or on the opposite side of the β-propeller, corresponding to the portions connecting the antiparallel β-strands. Among these more fluctuating domains, the most remarkable ones are those that were not resolved in the X-ray structure of the protein alone (PDB entry 1SNT)[5] and, in particular, the two mobile loops

dx.doi.org/10.1021/bi500249r | *Biochemistry* 2014, 53, 5343−5355

comprising helices α1 and α2, containing Asp 46 and Glu 111, respectively (Figure 1).

The calculation of secondary structure components (Figure 9A) by means of the DSSP software shows that at 300 K no

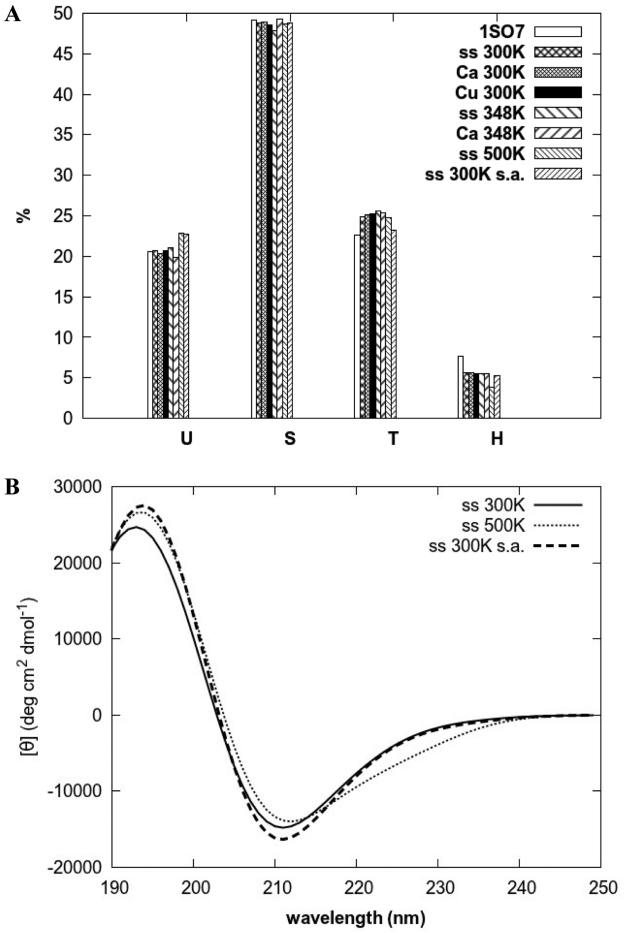

Figure 9. (A) Percent of four secondary structure types in the different MD simulations of human cytosolic sialidase NEU2: U for unordered, S for sheet, T for turn, and H for helix. (B) CD spectra (mean residue ellipticity, MRE, vs wavelength) calculated with PROTEIN over the trajectories of the MD simulations of NEU2 in *ss* solution at 300 and 500 K, and under simulated annealing (s.a.) conditions at 300 K. For further information, see the text.

significant variation occurs with respect to the crystal structure. With respect to the analysis of Table 1 and Figure 6, where the same information is deduced from CD spectra, these results indicate a larger fraction of S and T and a smaller fraction of U and H, especially when compared to the analysis of spectra in solution. This implies that with respect to the secondary structure information derived from CD spectra by using current methods,[13,15−18] a qualitative agreement, rather than a strict correspondence, should be sought. Further insight should be obtained by comparing calculated and experimental CD spectra. Let us first examine the CD spectrum obtained at 300 K (Figure 9B) as an average over 1000 conformations evenly spaced in the interval between 30 and 50 ns of the *ss* trajectory. CD spectra averaged over subsets of these conformations show very small differences, confirming that the secondary structure is extremely stable under the simulation conditions used. On the other hand, the calculated spectra differ from the corresponding experimental spectra (Figure 4) in two main aspects: (i) the double negative peak is not predicted by calculations, and (ii) the intensity of the whole spectrum is overestimated. By considering the other two calculated CD spectra of Figure 9B, only minor changes are observed for simulations at a higher temperature (500 K) or after simulated annealing (300 K, s.a.), as will be discussed below. This is true even when an algorithm (PROTPOL) is used to evaluate the CD spectrum that includes polarizability corrections[37−39] (see Figure SI1 of the Supporting Information, where, because of computational limits, just a few representative structures have been analyzed). Indeed, the effect of such contributions is expected to be relevant for molecules with a high content of poly(Pro)II secondary structure, which can be estimated to be <10% in this case and essentially independent of temperature (Table SI1 and Figure SI2 of the Supporting Information). These results suggest that, because of the well-known rigidity of the β-propeller structure,[45,47] MD simulations in the approach presented here cannot account for all details of CD measurements, while they may provide useful information concerning some feature of the enzyme behavior in the presence of divalent cations,[8] as well as the enzyme/substrate recognition mechanism.[5]

With regard to divalent cations, while it has been shown that their presence affects the biological activity[8] and the CD spectra (Figures 4 and 5), the detailed mechanism of their interaction with NEU2 is not known. In particular, it has been suggested that cations could enter into the acidic hole opposite the active site, because of favorable electrostatic interactions.[5] It is then interesting to analyze, using MD simulations of solutions containing Ca^{2+} and Cu^{2+} ions, the average numbers of cations within 10 Å of the center of mass of each residue, as shown in Figure 10A at 300 K.

The first observation is that Ca^{2+} ions have a remarkably higher probability of establishing contacts with NEU2 than Cu^{2+} ions. It is intriguing to note the fact that the general appearance of the experimental CD spectra in the presence of Ca^{2+} ions is different from those in PB, while in the presence of Cu^{2+} ions, there is a substantial identity (however, in the latter case, the transition temperature changes noticeably). Again, calculated CD spectra do not reproduce the observed differences among the three cases (Figure SI3 of the Supporting Information). Noteworthy is the fact that the effect of the divalent cations on the enzyme activity is quite different (Figure 7). Looking in more detail at the data of Figure 10, we can identify the most probable sites of interaction of Ca^{2+} ions in the segments of residues 46−50, 107−111, 225−228, 249−253, 280−290, and 357−361 of the sequence, where negatively charged residues such as Asp and Glu are present with side chains exposed to the solvent, but not in the acidic hole opposite the active site. It is particularly interesting to notice the peaks around residues Asp 46 and Glu 111, in connection with their role in DANA/substrate coordination.[5,11] In this perspective, Figure 10B shows that Ca^{2+} ions affect the distance distribution of Glu 111 with respect to Tyr 334 (see also Figures 1A and 2A). As deduced by comparison with distances obtained from the X-ray structures of PDB entries 1SO7 and 1VCU reported as dotted vertical lines in the figure, loop α2 is essentially in its open position in the presence of Ca^{2+}, while both in *ss* and in the presence of Cu^{2+} ions, comparable populations of the open and closed NEU2 conformations are present. Conversely, Asp 46 remains in an open position, although the presence of the divalent cations slightly shifts the residue toward the closed position. Overall, it is tempting to speculate that the slight activating/protecting effect exerted by Ca^{2+} on enzyme activity could be somehow linked to its effect exerted on the Glu

dx.doi.org/10.1021/bi500249r | *Biochemistry* 2014, 53, 5343−5355

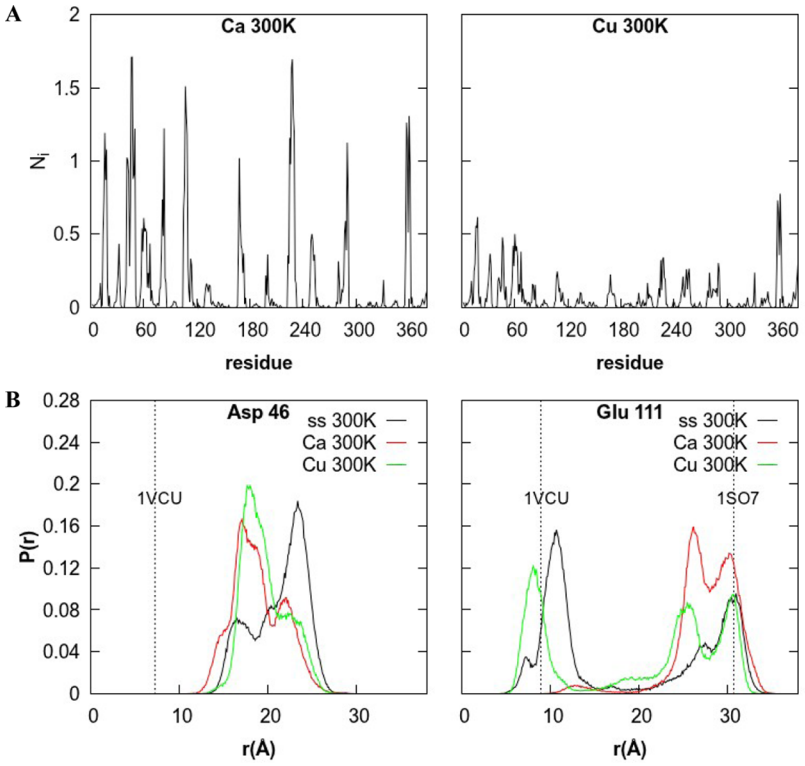

Figure 10. (A) Average number of Ca^{2+} ions within 10 Å of the center of mass of each residue over 250 ns of cumulative MD simulations of NEU2 (left) and average number of Cu^{2+} ions within 10 Å of the center of mass of each residue over 200 ns of MD simulations of NEU2 (right). (B) Superimposed probability density distributions of the distance between the Cγ (CG) atom of Asp 46 and the oxygen atom of the OH group of Tyr 334 in *ss* solution and in the presence of Ca^{2+} and Cu^{2+} ions, as from MD simulations of NEU2 (left), and superimposed probability density distributions of the distance between the Cδ atom of Glu 111 and the oxygen atom of the OH group of Tyr 334 in *ss* solution in the presence of Ca^{2+} and Cu^{2+} ions, as from MD simulations of NEU2 (right).

111 position. A more complete explanation of this mechanism is beyond the scope of this work and requires the simulations of the protein in the presence of natural ligands.

As mentioned above, MD simulations of NEU2 at 300 K and then at 348 and 358 K, namely, ∼20 and ∼30 K above the experimentally observed transitions in the CD spectra, respectively, do not provide an overall shape of the molecule different from that found by X-ray analysis. Apart from an expected increased overall fluctuation of the structure, no significant structural changes were observed during several simulations conducted from 50 to 100 ns, both for *ss* and in the presence of Ca^{2+}, except that in the latter case the closed conformation of loop α2 is observed, contrary to the 300 K case (data not shown).

To extend our exploration of NEU2 beyond the conformational space accessible to MD during the time allowed by our computational resources, we simulated the system at 500 K for 100 ns. Such a high value, although unphysical in principle, is useful for accelerating the conformational sampling, as was also recently pointed out by Euston.[48] As a matter of fact, the solvent did not display any abrupt density change during the simulation time. It is remarkable that even under these extreme conditions and over 100 ns MD simulations, the secondary structure remains essentially the same as in the low-temperature simulations (Figure 9A) and the calculated CD spectra (300, 500, and 300 K, s.a.) obtained using PROTEIN (Figure 9B) exhibit only slight differences. In addition, calculations of CD spectra using PROTPOL are reported in Figure SI4 of the Supporting Information.

However, some interesting local structural features of NEU2 emerge from the analysis of the MD trajectory at this high temperature. Comparison of *B* factors per residue between 500 and 300 K (Figure 11A) shows, as expected, that the largest motions are mainly located in the loops connecting the antiparallel β-strands of the β-propeller, as well as at the C-terminus of the polypeptide, indicating the more mobile portions of the molecule.

High mobility also characterizes the residues of the active site, whose organization is briefly summarized here. On the basis of X-ray studies, the competitive inhibitor DANA interacts with several residues: it enters the active site and undergoes either electrostatic or hydrophobic interactions with eight residues of the catalytic crevice (Arg 21, Met 85, Tyr 179, Tyr 181, Leu 217, Arg 237, Arg 304, and Tyr 334), while the two loops containing helices α1 and α2 that appear disordered in the apo form (PDB entry 1SNT) become ordered and bend over the active site (PDB entry 1VCU) with Asp 46 and Glu 111 forming two additional hydrogen bonds with the C4 hydroxyl group and glycerol tail of DANA, respectively[5,11] (Figures 1 and 2).

Moreover, using MD simulations, the overall geometry of the active site can be inspected by analyzing distributions of distances between the OH group of Tyr 334, localized in the active site bottom below C2 of the substrate, and the side chain atoms of the other residues involved in DANA coordination (Figure 11B).

Comparison of the patterns at 300 and 500 K reveals that the probability distribution of distances broadens considerably and in three cases, namely, Asp 46, Glu 111, and Arg 304, significantly extends beyond 20 Å. In particular, Arg 304, belonging to the Arg triad responsible for substrate recognition,[5,10] exhibits a well-

dx.doi.org/10.1021/bi500249r | *Biochemistry* 2014, 53, 5343−5355

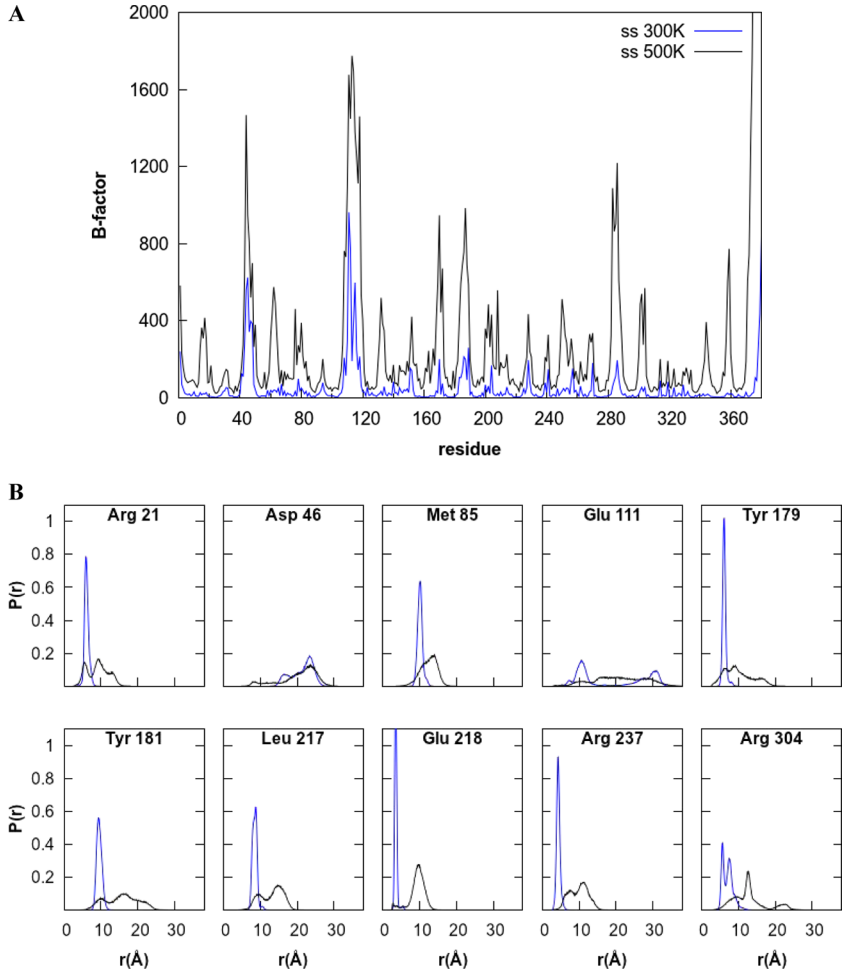

Figure 11. (A) *B* factor (square angstroms) per residue as evaluated from two 100 ns MD simulations in *ss* solution at 300 K (blue) and and 500 K (black). (B) Superimposed probability density distributions of the distances between atoms in relevant residues of the active site crevice of NEU2 and the oxygen atom of the OH group of Tyr 334, as evaluated from 100 ns MD simulations conducted at 300 K (blue) and 500 K (black). The atoms from which the distances are measured are (following the standard PDB naming conventions) Arg 21 NH1, Asp 46 CG, Met 85 SD, Glu 111 CD, Tyr 179 OH, Tyr 181 OH, Leu 217 CG, Glu 218 OE1, Arg 237 NH1, and Arg 304 CZ.

defined separate double peak centered at ∼23 Å. Full analysis of Figure 11B points out also the high mobility of residues Asp 46 and Glu 111, as evidenced by the very broad distributions of their distances from Tyr 334. In particular, the distribution of Glu 111 is broader than that of Asp 46, and this is related to the fact that the loop containing helix α2 is longer than that containing helix α1, allowing larger-amplitude motions. Moreover, the distance distribution of Glu 111 is essentially bimodal at 300 K, corresponding to its position in the open and closed conformation of NEU2, without significant intermediate states. From the time evolution of the distance between Tyr 334 and Glu 111, as well as with Asp 46, we notice that, according to MD simulations, the motions of these loops typically occur over times on the order of 20−30 ns, so that a transition from the open to closed form or vice versa may occur just once or twice or may not even occur in a time span of 50−100 ns. (Better statistics for these events are obtained here by means of multiple simulations of the same systems, starting from different initial conditions.)

In view of the special role of Arg 304, interesting insight is gained by looking at the superposition of the two antiparallel β-strands linked by the loop bearing Arg 304 (for details, see Figure 1B) of PDB entry 1SO7, the maltose-NEU2 crystal structure used as a starting point for the MD simulations at 500 K, with the corresponding positions found in three representative structures calculated at 25, 70, and 100 ns at 500 K (Figure 12A). MD simulations show that the loop bearing Arg 304 undergoes a large conformational change, resulting in a gradual movement of the side chain of this residue from its original position inside the active site crevice to outside.

Because, as already mentioned, Arg 304 belongs to the Arg triad that binds the carboxylate group common to all sialic acids,[5,10] this transition was investigated in two respects: (i) the mechanism of rearrangement of the HB network and (ii) the reversibility of the phenomenon. The most relevant HBs of Arg 304 with the surrounding residues are analyzed in Figure 12B, which indicates that the Arg 304 backbone is involved in HB with the corresponding portion of Cys 332 at the beginning of the simulations. Then until roughly 50 ns the distal portion of the Arg 304 side chain establishes an additional HB with the corresponding portion of Asp 358 and the carbonyl group of Cys 332. In the following time interval, until roughly 90 ns, the HB network involves the side chains of Arg 304, Ser 331, and Glu 355. Finally, roughly in the last 10 ns, when Arg 304 is completely outside the active site, the carboxyl group of the Asp 306 side chain establishes an HB with the side chain of Arg 304, whereas the backbone of His 300 interacts with the corresponding

dx.doi.org/10.1021/bi500249r | *Biochemistry* 2014, 53, 5343−5355

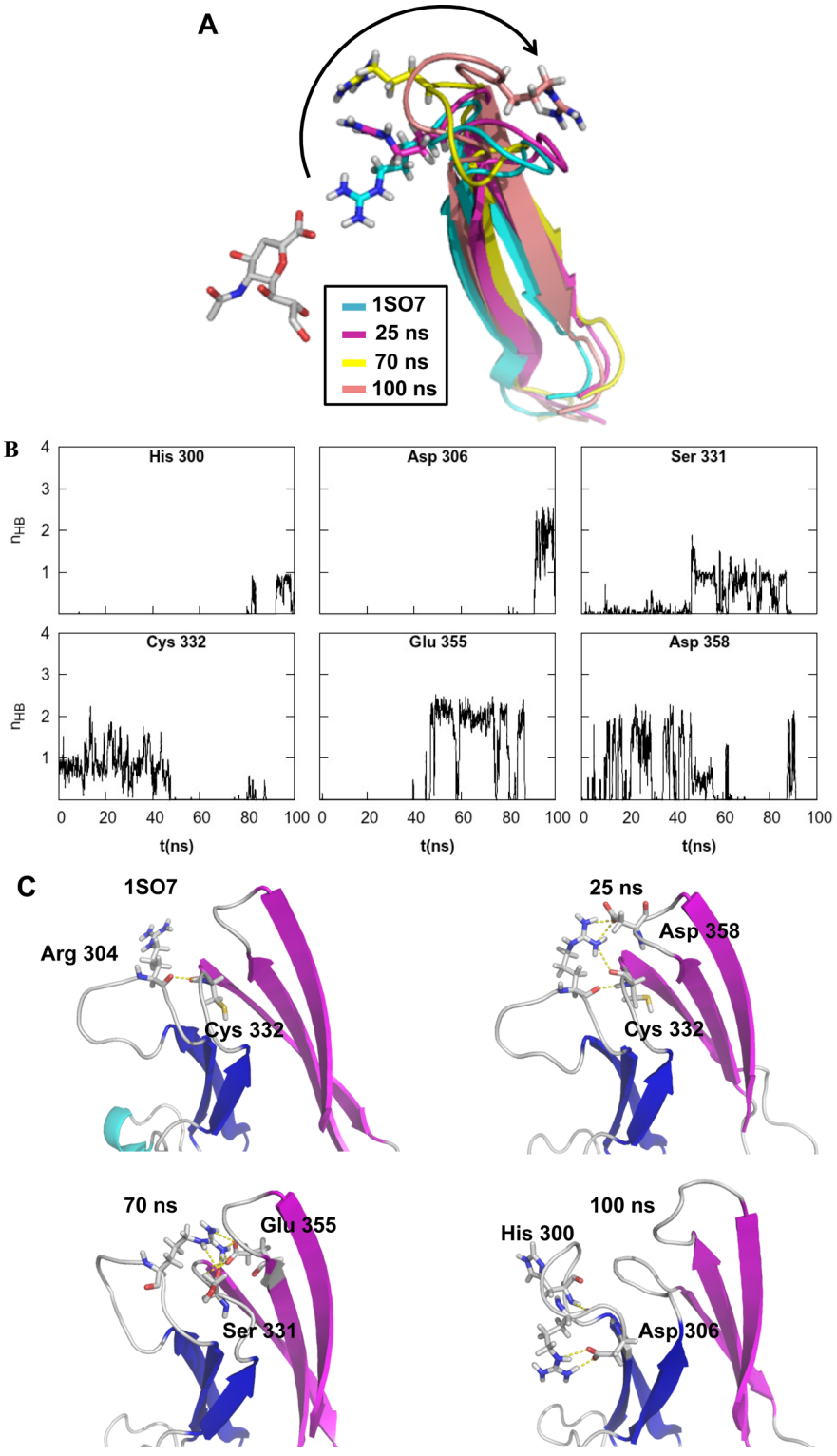

Figure 12. (A) Structure comparison of the portion of NEU2 bearing Arg 304 as evaluated from MD simulations at 500 K. Structures at the beginning (PDB entry 1SO7) and 25, 70, and 100 ns are represented as ribbon diagrams with different colors and encompass residues from Ser 288 to Pro 315. The Arg 304 side chain is shown in a stick representation, and the position of the competitive inhibitor DANA is located as in the X-ray structure of PDB entry 1VCU. (B) Time evolution of HBs between Arg 304 and some surrounding residues, as evaluated from MD simulations of NEU2 at 500 K in *ss*. Values are reported as running averages over 200 ps. (C) Structural representation of the HB network as deduced from panel B. The four structures are represented as ribbon diagrams, from Ser 288 to Thr 369, using the same color code that is used in panels A and B of Figure 1. Three strands of blade V, namely B−D, are colored dark blue, and the first three strands of blade VI are colored magenta. Side chains and backbones of the residues involved in the HB network are represented as sticks. HBs are depicted as dashed yellow lines.

dx.doi.org/10.1021/bi500249r | *Biochemistry* 2014, 53, 5343−5355

portion of the basic residue. The temporal sequence of these HB networks involving Arg 304 during MD simulations at 500 K is depicted in Figure 12C.

The reversibility of this phenomenon has been checked in two simulations. In the first, the temperature was gradually decreased to 348 K in a time span of roughly 60 ns, at the end of which the temperature was kept constant for 100 ns; in the second, starting from the end of the first one, the temperature was decreased to 300 K in roughly 20 ns and the system was then simulated for 50 ns at a constant temperature. Under these conditions, the position of Arg 304 was never observed to return inside the active site. It is tempting to speculate that Arg 304 mobility could represent one of the factors involved in the observed lability of the enzyme catalytic power, which has been known since the beginning of the studies of animal sialidases.[1]

SUMMARY AND CONCLUSIONS

In this work, cytosolic sialidase NEU2 has been studied by different experimental and computational methods, encompassing CD, IR, and MD. In the solid state, CD and IR are in agreement with the previous structural analysis based on X-ray diffraction, which had defined the protein as a β-propeller with six quartets of β-strands paired with an antiparallel topology, and connected to each other in various ways, i.e., sometimes by β-turns or by unordered coils or by loops containing α-helices. The role of α-helices is magnified, for not fully understood reasons, in solution, as evidenced by CD. MD has allowed us to predict qualitatively a CD spectrum, which, though being of the correct order of magnitude and gross overall shape, does not however exhibit the characteristic negative doublet found here and in all CD spectra of α-structures. Besides, the experimental CD spectra of NEU2 exhibit well-defined changes, which may be related to conformational transitions in the same temperature range where the enzymatic activity decreases due to heat inactivation. Moreover, in the presence of divalent cations, changes in the CD spectra, as well as in biochemical activity, are detectable, compared to those in the presence of PB.

However, the fact that sialidase activity is labile even at room temperature, a point at which no changes in the CD signal are noticed, suggests that local conformational variations may impair NEU2 enzyme activity. MD simulations were useful for gaining insight into local structural features. Indeed, MD, while confirming the very rigid overall β-propeller structure of NEU2, provides evidence of the high mobility of the loops bearing the helices α1 and α2, allowing estimation of the amplitude and time scale of their motions. In the presence of divalent cations, Ca^{2+} and Cu^{2+}, the main sites of protein−ion interaction are identified, and a tendency of Ca^{2+} ions to favor the open position of the loop containing helix α2 is observed. In a simulated annealing process, involving an increase in temperature from 300 to 500 K and a subsequent slow descent to the initial temperature, one of the Arg triad residues, Arg 304, was observed to move outside the active site through a rearrangement of the local network of HBs and maintained this position for all the remaining simulation time, which was much longer than the transition time. This finding could help explain the labile nature of the enzyme activity typical of mammalian sialidases.

ASSOCIATED CONTENT

Supporting Information

CD spectra of NEU2 calculated on the basis of MD trajectories for representative structures at 300 K using PROTPOL (Figure SI1), percent of secondary structures calculated from MD structures (Table SI1), time evolution of poly(Pro)II percent in NEU2 at 300 and 500 K, as of MD simulations (Figure SI2), comparison of calculated CD spectra of NEU2 in the presence of divalent ions with corresponding calculations in *ss* condition and using PROTEIN (Figure SI3), and calculated CD spectra of NEU2 on the basis of MD trajectories for representative structures at 500 K using PROTPOL (Figure SI4). This material is available free of charge via the Internet at http://pubs.acs.org.

AUTHOR INFORMATION

Corresponding Author

*E-mail: eugenio.monti@unibs.it.

Author Contributions

E.M., G.L., E.C., F.G., S.L.F., R.W.W., and S.A. conceived and designed the experiments. A.M. and P.F. produced and purified recombinant NEU2. G.B., G.L., and E.C. conducted the IR and CD experiments. F.G. and S.L.F. conducted MD simulations. E.M., G.L., F.G., S.L.F., R.W.W., and S.A. wrote the paper.

Funding

We thank Italian MIUR (Ministero dell'Istruzione, dell'Università e della Ricerca) for financial support. This work was partly supported by Regione Lombardia and a Network Enable Drug Discovery-NEDD grant to E.M.

Notes

The authors declare no competing financial interest.

ACKNOWLEDGMENTS

We thank CILEA (Consorzio Interuniversitario Lombardo Elaborazione Automatica) for access to their computational facilities.

REFERENCES

(1) Saito, M., and Yu, R. K. (1995) Biochemistry and Function of Sialidases. In *Biology of the Sialic Acids* (Rosenberg, A., Ed.) pp 261−313, Plenum Press, New York.

(2) Giacopuzzi, E., Bresciani, R., Schauer, R., Monti, E., and Borsani, G. (2012) New insights on the sialidase protein family revealed by a phylogenetic analysis in metazoa. *PLoS One 7*, e44193.

(3) von Itzstein, M. (2007) The war against influenza: Discovery and development of sialidase inhibitors. *Nat. Rev. 6*, 967−974.

(4) Taylor, G. (1996) Sialidases: Structures, biological significance and therapeutic potential. *Curr. Opin. Struct. Biol. 6*, 830−837.

(5) Chavas, L. M., Tringali, C., Fusi, P., Venerando, B., Tettamanti, G., Kato, R., Monti, E., and Wakatsuki, S. (2005) Crystal structure of the human cytosolic sialidase Neu2. Evidence for the dynamic nature of substrate recognition. *J. Biol. Chem. 280*, 469−475.

(6) Copley, R. R., Russell, R. B., and Ponting, C. P. (2001) Sialidase-like Asp-boxes: Sequence-similar structures within different protein folds. *Protein Sci. 10*, 285−292.

(7) Quistgaard, E. M., and Thirup, S. S. (2009) Sequence and structural analysis of the Asp-box motif and Asp-box β-propellers; a widespread propeller-type characteristic of the Vps10 domain family and several glycoside hydrolase families. *BMC Struct. Biol. 9*, 46.

(8) Tringali, C., Papini, N., Fusi, P., Croci, G., Borsani, G., Preti, A., Tortora, P., Tettamanti, G., Venerando, B., and Monti, E. (2004) Properties of recombinant human cytosolic sialidase HsNEU2. The enzyme hydrolyzes monomerically dispersed GM1 ganglioside molecules. *J. Biol. Chem. 279*, 3169−3179.

(9) Albouz-Abo, S., Turton, R., Wilson, J. C., and von Itzstein, M. (2005) An investigation of the activity of recombinant rat skeletal muscle cytosolic sialidase. *FEBS Lett. 579*, 1034−1038.

(10) Buschiazzo, A., and Alzari, P. M. (2008) Structural insights into sialic acid enzymology. *Curr. Opin. Chem. Biol. 12*, 565−572.

(11) Mozzi, A., Mazzacuva, P., Zampella, G., Forcella, M. E., Fusi, P. A., and Monti, E. (2012) Molecular insight into substrate recognition by human cytosolic sialidase NEU2. *Proteins 80*, 1123−1132.
(12) Brahms, S., and Brahms, J. (1980) Determination of protein secondary structure in solution by vacuum ultraviolet circular dichroism. *J. Mol. Biol. 138*, 149−178.
(13) Provencher, S. W., and Glöckner, J. (1981) Estimation of globular protein secondary structure from circular dichroism. *Biochemistry 20*, 33−37.
(14) Greenfield, N. J. (1996) Methods to estimate the conformation of proteins and polypeptides from circular dichroism data. *Anal. Biochem. 235*, 1−10.
(15) Johnson, W. C. (1999) Analyzing protein circular dichroism spectra for accurate secondary structures. *Proteins 35*, 307−312.
(16) Sreerama, N., and Woody, R. W. (2000) Estimation of protein secondary structure from circular dichroism spectra: Comparison of CONTIN, SELCON, and CDSSTR methods with an expanded reference set. *Anal. Biochem. 287*, 252−260.
(17) Greenfield, N. J. (2006) Using circular dichroism spectra to estimate protein secondary structure. *Nat. Protoc. 1*, 2876−2890.
(18) Woody, R. W. (2012) Electronic Circular Dichroism of Proteins. In *Comprehensive Chiroptical Spectroscopy* (Berova, N., Polavarapu, P. L., Nakanishi, K., and Woody, R. W., Eds.) pp 474−498, Wiley, Hoboken, NJ.
(19) Merten, C., Kowalik, T., and Hartwig, A. (2008) Vibrational circular dichroism spectroscopy of solid polymer films: Effects of sample orientation. *Appl. Spectrosc. 62*, 901−905.
(20) Pronk, S., Pall, S., Schulz, R., Larsson, P., Bjelkmar, P., Apostolov, R., Shirts, M. R., Smith, J. C., Kasson, P. M., van der Spoel, D., Hess, B., and Lindahl, E. (2013) GROMACS 4.5: A high-throughput and highly parallel open source molecular simulation toolkit. *Bioinformatics 29*, 845−854.
(21) Sorin, E. J., and Pande, V. S. (2005) Exploring the helix-coil transition via all-atom equilibrium ensemble simulations. *Biophys. J. 88*, 2472−2493.
(22) Hornak, V., Abel, R., Okur, A., Strockbine, B., Roitberg, A., and Simmerling, C. (2006) Comparison of multiple Amber force fields and development of improved protein backbone parameters. *Proteins 65*, 712−725.
(23) DePaul, A. J., Thompson, E. J., Patel, S. S., Haldeman, K., and Sorin, E. J. (2010) Equilibrium conformational dynamics in an RNA tetraloop from massively parallel molecular dynamics. *Nucleic Acids Res. 38*, 4856−4867.
(24) Berman, H. M., Westbrook, J., Feng, Z., Gilliland, G., Bhat, T. N., Weissig, H., Shindyalov, I. N., and Bourne, P. E. (2000) The Protein Data Bank. *Nucleic Acids Res. 28*, 235−242.
(25) Guex, N., and Peitsch, M. C. (1997) SWISS-MODEL and the Swiss-PdbViewer: An environment for comparative protein modeling. *Electrophoresis 18*, 2714−2723.
(26) Cantor, C. R., and Schimmel, P. R. (1980) Part I: The Conformation of Biological Molecules. In *Biophysical Chemistry*, W. H. Freeman Publishers and Co., San Francisco.
(27) Babu, C. S., and Lim, C. (2006) Empirical force fields for biologically active divalent metal cations in water. *J. Phys. Chem. A 110*, 691−699.
(28) Parrinello, M., and Rahman, A. (1981) Polymorphic Transitions in Single-Crystals: A New Molecular-Dynamics Method. *J. Appl. Phys. 52*, 7182−7190.
(29) Nose, S., and Klein, M. L. (1983) Constant Pressure Molecular-Dynamics for Molecular Systems. *Mol. Phys. 50*, 1055−1076.
(30) Hess, B., Bekker, H., Berendsen, H. J. C., and Fraaije, J. G. E. M. (1997) LINCS: A linear constraint solver for molecular simulations. *J. Comput. Chem. 18*, 1463−1472.
(31) Kabsch, W., and Sander, C. (1983) Dictionary of protein secondary structure: Pattern recognition of hydrogen-bonded and geometrical features. *Biopolymers 22*, 2577−2637.
(32) Joosten, R. P., te Beek, T. A., Krieger, E., Hekkelman, M. L., Hooft, R. W., Schneider, R., Sander, C., and Vriend, G. (2011) A series of PDB related databases for everyday needs. *Nucleic Acids Res. 39*, D411−D419.
(33) Gangemi, F., Longhi, G., Abbate, S., Lebon, F., Cordone, R., Ghilardi, G. P., and Fornili, S. L. (2008) Molecular dynamics simulation of aqueous solutions of 26-unit segments of p(NIPAAm) and of p(NIPAAm) "doped" with amino acid based comonomers. *J. Phys. Chem. B 112*, 11896−11906.
(34) Tinoco, I. J. (1962) Theoretical Aspects of Optical Activity Part Two: Polymers. In *Advances in Chemical Physics*, pp 113−160, Interscience Publishers, New York.
(35) Bayley, P. M., Nielsen, E. B., and Schellman, J. A. (1969) The rotatory properties of molecules containing two peptide groups: Theory. *J. Phys. Chem. 73*, 228−243.
(36) Koslowski, A., Sreerama, N., and Woody, R. W. (2000) Theoretical Approach to Electronic Optical Activity. In *Circular Dichroism, Principles and Applications* (Berova, N., Nakanishi, K., and Woody, R. W., Eds.) 2nd ed., pp 55−96, Wiley-VCH, New York.
(37) Sreerama, N., and Woody, R. W. (2004) Computation and analysis of protein circular dichroism spectra. *Methods Enzymol. 383*, 318−351.
(38) Woody, R. W. (2009) Circular dichroism spectrum of peptides in the poly(Pro)II conformation. *J. Am. Chem. Soc. 131*, 8234−8245.
(39) Woody, R. W. (2010) A significant role for high-energy transitions in the ultraviolet circular dichroism spectra of polypeptides and proteins. *Chirality 22* (Suppl. 1), E22−E29.
(40) Humphrey, W., Dalke, A., and Schulten, K. (1996) VMD: Visual molecular dynamics. *J. Mol. Graphics 14*, 33−38.
(41) Chavas, L. M., Kato, R., Suzuki, N., von Itzstein, M., Mann, M. C., Thomson, R. J., Dyason, J. C., McKimm-Breschkin, J., Fusi, P., Tringali, C., Venerando, B., Tettamanti, G., Monti, E., and Wakatsuki, S. (2010) Complexity in influenza virus targeted drug design: Interaction with human sialidases. *J. Med. Chem. 53*, 2998−3002.
(42) Surewicz, W. K., and Mantsch, H. H. (1996) Infrared Absorption Methods for Examining Protein Structures. In *Spectroscopic Methods for Determining Protein Structures in Solution* (Havel, H. A., Ed.) pp 135−162, Wiley-VCH, New York.
(43) Sarver, R. W., Jr., and Krueger, W. C. (1991) An infrared and circular dichroism combined approach to the analysis of protein secondary structure. *Anal. Biochem. 199*, 61−67.
(44) Sarver, R. W., Jr., and Krueger, W. C. (1991) Protein secondary structure from Fourier transform infrared spectroscopy: A data base analysis. *Anal. Biochem. 194*, 89−100.
(45) Fulop, V., and Jones, D. T. (1999) β propellers: Structural rigidity and functional diversity. *Curr. Opin. Struct. Biol. 9*, 715−721.
(46) Fuxreiter, M., Magyar, C., Juhasz, T., Szeltner, Z., Polgar, L., and Simon, I. (2005) Flexibility of prolyl oligopeptidase: Molecular dynamics and molecular framework analysis of the potential substrate pathways. *Proteins 60*, 504−512.
(47) Chen, C. K., Chan, N. L., and Wang, A. H. (2011) The many blades of the β-propeller proteins: Conserved but versatile. *Trends Biochem. Sci. 36*, 553−561.
(48) Euston, S. R. (2013) Molecular dynamics simulation of the effect of heat on the conformation of bovine β-lactoglobulin A: A comparison of conventional and accelerated methods. *Food Hydrocolloids 30*, 519−530.